Using a High-Frequency Fluorescent Oxygen Probe in Atmospheric Eddy Covariance Applications

ANDREAS ANDERSSON, ANNA RUTGERSSON, AND ERIK SAHLÉE

Program for Air, Water and Landscape Sciences, Department of Earth Sciences, Uppsala University, Uppsala, Sweden

(Manuscript received 28 November 2013, in final form 11 July 2014)

ABSTRACT

During the years 2010–13, atmospheric eddy covariance measurement of oxygen was performed at the marine site Östergarnsholm in the Baltic Sea. The fast response optode Microx TX3 was used with two different types of tapered sensors. In spite of the increased lifetime, the optical isolated sensor is limited by the slower response time and is unsuitable for ground-based eddy covariance measurements. The sensor without optical isolation shows a $-2/3$ slope within the inertial subrange and attains sufficient response time and precision to be used in air–sea applications during continuous periods of 1–4 days. Spectral and cospectral analysis shows oxygen measured with the nonoptical isolated sensor to follow the same shape as for CO_2 and water vapor when normalized. The sampling rate of the Microx TX3 is 2 Hz; however, the sensor was found to have a limited response and resolution, yielding a flux loss in the frequency range $f > 0.3$ Hz. This can be corrected for by applying cospectral similarity simultaneously using measurements of latent heat as the reference signal. On average the magnitude of the cospectral correction added 20% to the uncorrected oxygen flux during neutral atmospheric stratification.

1. Introduction

Air–sea exchange of oxygen is an area of increasing scientific interest. Oxygen in the ocean is of crucial importance, as it is strongly linked to both the carbon dioxide and nitrogen cycles (Arrigo 2005; Keeling et al. 2010) and is a key component in eutrophication (Karlsson et al. 2002). In the fifth and latest assessment report from the Intergovernmental Panel on Climate Change (Stocker et al. 2013), it was concluded that the ocean has absorbed about 30% of the emitted anthropogenic carbon dioxide, causing ocean acidification. Variability of oxygen gives additional information about the carbon cycle, not contained in the variability of CO_2, due to the different reactivity and equilibrium time scale of oxygen and CO_2 (Körtzinger et al. 2008).

During the last decade, there has been increasing interest in oxygen minimum zones (OMZ). OMZ are zones in the water column typically 200–1000 m in depth where oxygen concentration is at its lowest and hypoxia occurs. OMZ constitute the main areas of nitrogen loss to the atmosphere via denitrification and anaerobic ammonium oxidation (Codispoti et al. 2001) and could also mitigate the ocean biological sequestration of atmospheric CO_2 (Paulmier et al. 2008). In the last few years, new evidence of expanding OMZ has been found in the tropical northeast Atlantic as a consequence of global warming (Stramma et al. 2008), capable of threatening the sustainability of pelagic fisheries and marine ecosystems (Stramma et al. 2012). Recently, the Surface Ocean Lower Atmosphere Study (SOLAS) launched a program related to OMZ as a key player to understand the nitrogen cycle and the role of the ocean in atmospheric greenhouse gas control. The oxygen concentration of these zones is very sensitive to changes in air–sea fluxes of oxygen and interior ocean advection; hence, dissolved oxygen is an important parameter for the understanding of the ocean's role in the earth's climate system (Joos et al. 2003). One major uncertainty of the ocean oxygen dynamics is the air–sea gas exchange. Therefore, measurements of oxygen fluxes across the air–sea surface are fundamental to the understanding of how the increased emissions of greenhouse gases—for

Denotes Open Access content.

Corresponding author address: Andreas Andersson, Department of Earth Sciences, Uppsala University, Villavägen 16, SE-752 36 Uppsala, Sweden.
E-mail: andreas.andersson@geo.uu.se

DOI: 10.1175/JTECH-D-13-00249.1

example, CO_2, CH_4, and NO_2—affect the global climate dynamics.

The most direct method to measure fluxes of gases across the air–sea interface is the eddy covariance method. This method is widely used within the meteorological community to determine, for example, fluxes of CO_2, and sensible and latent heat. Oxygen eddy covariance measurements in water have been performed successfully over the last decade in studying water–sediment exchange (e.g., Berg et al. 2003, 2009; Kuwae et al. 2006; Brand et al. 2008; McGinnis et al. 2008; Reimers et al. 2012; Chipman et al. 2012). Atmospheric eddy covariance measurements of oxygen have not previously been performed, since instrumentation with sufficient response time and resolution was not available.

The magnitude and direction of a gas flux at the air–sea interface is determined by the air–sea difference in partial pressure of the gas and by the efficiency of the transfer process (described by the transfer velocity). Traditionally, the air–sea fluxes of oxygen have been determined through mass balance techniques using the oxygen disequilibrium between the atmosphere and the surface ocean and using a wind-dependent expression for the transfer velocity (e.g., Stigebrandt 1991; McNeil et al. 2006; Kihm and Körtzinger 2010). Measurements of sparingly soluble gases such as CO_2 suggest linear, quadratic, or cubic dependencies of transfer velocity on wind speed (Liss and Merlivat 1986; Wanninkhof 1992; Wanninkhof and McGillis 1999; McGillis et al. 2004; Woolf 2005; McNeil and D'Asaro 2007). The relative importance of various processes for the air–sea exchange is still not fully understood (Garbe et al. 2014). In the low to intermediate wind speed regime, the primary driving mechanism is presumed to be near surface turbulence (e.g., Fairaill et al. 2000). Additionally, microwave breaking (Zappa et al. 2001), spray and bubbles (Woolf 1993, 1997), and water-side convection (Rutgersson et al. 2011) are of importance. The relative importance of different processes is expected to vary for gases of different solubility. Dimethyl sulfide (DMS) has shown less wind speed dependence than CO_2 for high winds (Blomquist et al. 2006). By introducing eddy covariance measurements of yet another gas with different solubility (oxygen), knowledge about transport processes could fundamentally increase.

Here we evaluate the potential use of the Microx TX3 oxygen sensor for eddy covariance applications, investigating whether when it meets the resolution and response requirements for eddy covariance measurements in atmospheric marine environments, it will be exposed to, for example, high humidity and possible sea salt loading. A sensor comparison between two types of tapered oxygen sensors is performed, where response time and signal quality are studied. We also investigate the validity of scalar similarity on oxygen, by comparing cospectra of oxygen with cospectra of carbon dioxide and humidity. Additionally, we present corrections that need to be applied prior to a final flux estimate.

2. Theory

a. *Microx TX3*

The fast response oxygen optode is the commercially available optode system Microx TX3 (PreSens Precision Sensing GmbH, Regensburg Germany). The sensor consists of a needle-type housing with an oxygen sensitive tip $<50\,\mu$m and a fiber optical cable to the Microx TX3; a photograph of the sensor and instrument is shown in Fig. 1. The Microx TX3 uses the luminescence lifetime technique, which was specially developed for very small fiber optic oxygen microsensors, to measure the partial pressure of oxygen. This technique works in the following manner: first, an indicator molecule is transferred from its ground state to the excited state. In the absence of oxygen, the indicator molecule returns to its ground state and luminescence is measured (reference measurement). In the presence of oxygen, collisions occur between the excited indicator molecules and oxygen; as a result, energy is transferred from the indicator molecule to the oxygen molecule and the measurable luminescence signal decreases. As an oxygen-dependent parameter, the Microx TX3 uses decay time τ defined as the time between the excited signal and the molecule emitted signal. In the presence of oxygen, the decay time τ_1 is shorter compared to the decay time in oxygen-free air τ_0. Hence, the time delay between the excited and the emitted signal can be represented by a phase angle ϕ. The concept of the phase angle shift as a function of oxygen content is described in the Stern Volmer equation (Stern and Volmer 1919)

$$1 + K_{sv}[O_2] = \frac{\tau_0}{\tau_1} = \frac{\tan\phi_0}{\tan\phi_1}, \tag{1}$$

where K_{sv} is the Stern Volmer constant, $[O_2]$ denotes the oxygen content (e.g., partial pressure), ϕ_0 is the phase angle in absence of oxygen, and ϕ_1 in the presence of oxygen. The oxygen content can then be determined from the phase angle shift instead of luminescence intensity. According to the manual (Loligo Systems 2005), no cross sensitivity exists for carbon dioxide (CO_2), hydrogen sulfide (H_2S), ammonia (NH_3), pH, any ionic species like sulfide (S_2^-), sulfate (SO_4^{2-}), chloride (Cl^-), or salinity. The instrument can be set to give the oxygen output signal in partial pressure (hPa), oxygen saturation (0%–50%) or air saturation (0%–250%). For atmospheric eddy covariance

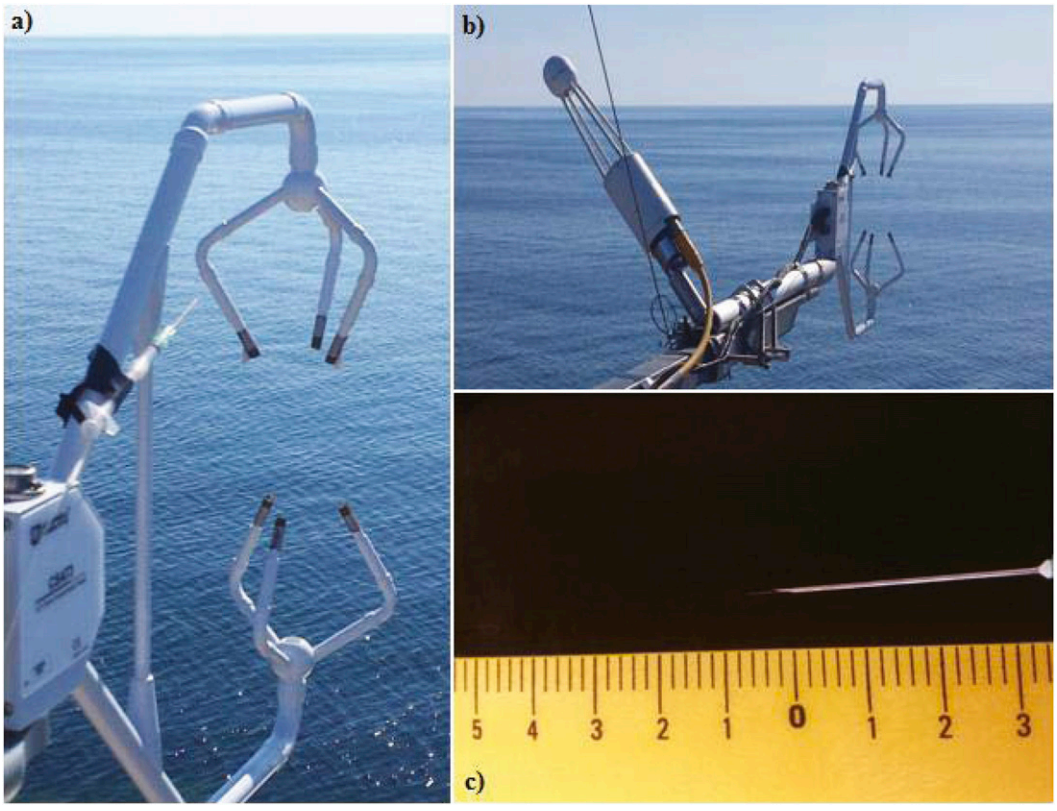

FIG. 1. (a) The EC system with a close-up of the NOI sensor mounted at the CSAT3 during P5, (b) the EC system used during P5 at the height of 27 m, and (c) a close-up of the NOI sensor tip.

applications, the oxygen partial pressure unit is preferred. The relative unit % air saturation is an air–water equilibrium unit, where 100% air saturation corresponds to a water surface in equilibrium with the normal volume content of oxygen in air (20.95%) at standard pressure (1013.25 hPa). The unit of % air saturation can be converted into dissolved oxygen O_2 (μmol L^{-1}) as

$$C_{O_2} = \frac{p_{atm} - p_w(T)}{p_n} \frac{\%\text{air-saturation}}{100} 0.2095\alpha(T)10^6 \frac{1}{V_m}, \quad (2)$$

where p_{atm} is the atmospheric pressure, p_n is the standard pressure, $p_w(T)$ is the saturation water vapor pressure at temperature T, V_m is the molar volume (22.414 L mol^{-1}) of oxygen, and $\alpha(T)$ is the Bunsen absorption coefficient for oxygen for a given temperature, assuming 100% relative humidity. For atmospheric measurements, assuming 100% relative humidity is not a valid approximation, since relative humidity is often significantly lower than 100%. This is why the actual water vapor pressure should be used instead of the saturation water vapor pressure. The Bunsen absorption coefficient is calculated using

$$\ln 10^3 \alpha(T) = \frac{8.553 \times 10^3}{T} + 23.78 \ln T - 160.8. \quad (3)$$

The Bunsen absorption coefficient determines the amount of oxygen that can be dissolved in water at a given water temperature.

A thermistor is connected to the Microx TX3 to correct for changes in quenching frequency due to temperature variations. This measurement may be bypassed by setting a fixed temperature, for which then the oxygen concentration is determined; this is, however, not the recommended setup when the best possible resolution is required. Here we test both setups, that is, using a fixed temperature and with the thermistor connected. The two types of tapered sensors used in this study are the optical isolated (OI) sensor and the nonoptical isolated (NOI) sensor. The NOI sensor has the advantage of a faster response time (t_{90}) < 0.5 s and accuracy of ± 1% air saturation compared to the OI sensor with $t_{90} <$ 1 s with the same accuracy, where t_{90} is the response time for 90% of the measured signal. The disadvantages of the NOI sensor compared to the OI sensor are the more fragile construction and a presumably larger signal drift as a result of faster photodecomposition of the oxygen

sensitive part, since it is more exposed to ambient light (Loligo Systems 2005). A signal drift will induce errors in the estimated flux if not corrected.

b. Eddy covariance method

The eddy covariance method is a direct measuring technique frequently used to determine turbulent fluxes. The technique uses the covariance between two simultaneously measured high-frequency signals. For vertical scalar fluxes, the covariance is calculated for vertical wind and a scalar measurement. The method is commonly used in micrometeorological studies to measure fluxes of momentum, heat, humidity, and CO_2 (Aubinet et al. 2012). The method requires a fast-responding instrument, typically 2 Hz or faster, with high precision. The required sampling frequency and resolution depends on a variety of factors, such as sampling height above ground, etc. For trace gases of high concentration and relatively small air–sea concentration gradients like oxygen, it becomes especially difficult to meet up with the typical required precision being of at least two orders of magnitude greater than that of the air–sea gradient of the scalar concentration (Wanninkhof et al. 2009). For higher latitudes oxygen saturation goes from being typically 0%–10% undersaturated in winter to become 10% oversaturated during spring bloom and early summer (Körtzinger et al. 2008). With a wind speed of 8 m s^{-1} and a 10% air–sea saturation difference, calculated fluxes are typically found within the range of 1–3 μmol m^{-2} s^{-1} (depending on SST and k_{660} parameterization). Because of the limited resolution of the Microx TX3, the eddy covariance measurements should be carried out when the air–sea oxygen gradient takes its highest values. The eddy covariance method relies on certain conditions that need to be fulfilled, such as a horizontally homogeneity and stationarity (see, e.g., Aubinet et al. 2012). With these conditions fulfilled, Reynolds decomposition can be applied and the scalar flux F_x expressed as

$$F_x = \overline{w'x'} + \overline{w}\,\overline{x}, \tag{4}$$

where x denotes the concentration of any scalar, such as CO_2, O_2, or humidity; w is the vertical wind component; and the primes represent a deviation from the mean value and the overbar represents the mean value. The first term on the right-hand side denotes the turbulent flux. The second term on the right-hand side is often neglected, with the motivation that the mean vertical wind component becomes zero after a coordinate rotation (tilt correction). This, however, is not a good assumption for all scalar fluxes, since the measured scalar density is affected by the density variations of temperature and humidity, causing a contribution to the mean vertical velocity. This can be corrected for on the raw signal or in the postprocessing using the Webb–Pearman–Leuning (WPL) correction (Webb et al. 1980) and is further discussed in section 4b(1).

c. Spectra and cospectra theory

Energy spectrum $E(k)$ relates the size of turbulent eddies in terms of wavenumber k to the energy of the specified quantity like humidity, CO_2, O_2, and other scalars. Following the Kolmogorov theory, the energy spectra within the inertial subrange can be described as a function of the dissipation rate ε and the wavenumber in the x direction:

$$E(k) = \alpha_k \varepsilon^{2/3} k^{-5/3}, \tag{5}$$

where α_k is the Kolmogorov constant, which for u is equal to 0.52, around 0.8 for temperature and humidity (Högström 1996). For CO_2, α_k has been suggested to have values between 0.78 and 0.89 (Ohtaki 1982; Verma and Anderson 1984). However, a recent study (Norman et al. 2012) suggested α_k for CO_2 equal to 0.68. For point measurements the energy spectra are usually expressed in terms of frequency n instead of wavenumber k. By applying the Taylor hypothesis, the wavenumber can be expressed in terms of mean wind velocity u and n. Multiplying by frequency the energy spectra for the horizontal wind component in the inertial subrange then follows the equation

$$nS_u(n) = \frac{\alpha_k}{2\pi^{2/3}} \varepsilon^{2/3} n^{-2/3} u^{2/3}. \tag{6}$$

Thus, theoretically $\log[nE(n)]$ should follow a $-2/3$ slope within the inertial subrange when shown against $\log(n)$. As shown by Kaimal et al. (1972) for the three wind components and temperature, and later on for CO_2 and humidity (Ohtaki and Matsui 1982; Ohtaki 1985; Anderson and Verma 1985), power spectra follow the Kolmogorov theory, showing a slope close to $-2/3$ within the inertial subrange.

The cospectrum essentially gives information about which sizes of eddies contribute to the flux. In a representation with a linear y axis and the frequency along a logarithmic x axis, the area beneath the curve is proportional to the flux. The scalar flux F_x may then be determined by computing the integral of the cospectrum (e.g., Wyngaard 2010):

$$F_x = \int_{-\infty}^{\infty} C_{wx}(n)\, dn = \overline{w'x'}. \tag{7}$$

Wyngaard and Cote (1972) found nC_{wu} and nC_{wt} to collapse in a $-4/3$ slope (Wyngaard and Cote 1972) within the inertial subrange, seen also for nC_{wq} and

TABLE 1. Dataset and setup during the five field campaigns including date for field campaign, hours with data (n), deployment height of the EC system (z), and the sensor type (ST) used for the respective period.

Period	Period of data	n	z	ST
P1	1 Jul 2010	7	10	OI
P2	30 Jun 2011–1 Jul 2011	18	27	NOI
P3	18–22 Apr 2012	83	27	NOI
P4	29 Aug 2012–4 Sep 2012	134	27	NOI
P5	19–24 Jun 2013	118.5	27	NOI

TABLE 2. Atmospheric conditions during the field campaigns with the atmospheric stability range (z/L), the average wind stress defined as $u_* = \sqrt{-\overline{u'w'}}$, wind speed range ($\mathrm{m\,s^{-1}}$), and the SL duration (h), estimated by inspection of the ratio σ_o/O_*.

Period	$(z/L)_{\text{range}}$	u_*	U_{range}	SL
P1	(−0.025)–(0.01)	0.10	2.4–5.0	>12
P2	(3.3×10^{-4})–(0.7)	0.16	0.9–5.7	>18
P3	(−0.04)–(0.014)	0.28	1.2–13.2	26
P4	(0.04)–(−0.05)	0.31	5.1–10.5	62
P5	(−0.02)–(0.04)	0.21	1.1–14.2	75

$nC_{\mathrm{wCO_2}}$ in Sahlée et al. (2008). Here spectra and cospectra are calculated in a similar way to Kaimal et al. (1972), consisting of 21 points from 20-Hz data, each representing a mean spectra estimate for the specific frequency range. Energy spectra and cospectra are normalized with its respective variance, σ_x^2, and flux $\overline{w'x'}$, respectively.

3. Site and instrument setup

a. Site description

The site used for the oxygen measurements is located on a small island east of Gotland in the Baltic Sea. A 30-m tower is located at the southern tip of the island with the base 1 ± 0.5 m above mean sea level. The tower is equipped with both slow response instruments for profiles and high-frequency instruments for turbulent fluxes. The fluxes of momentum, sensible heat, and latent heat are shown to represent open sea conditions for wind directions (WD) 80° < WD < 210° (Högström et al. 2008), while fluxes of CO_2 are shown to represent open sea conditions for wind direction 80° < WD < 160° (Rutgersson et al. 2008). Data from the site have been used for numerous studies on varies aspects on air–sea interaction and gas exchange (e.g., Rutgersson and Smedman 2010; Smedman et al. 1999). A more detailed description of the site and instrument setup can be found in, for example, Rutgersson et al. (2008).

b. Instrumental setup

The Microx TX3 was used in two different eddy covariance systems during the years 2010–13; see Table 1 for descriptions of the setups and measuring periods (P1–P5). For P1–P4 (2010–12), the eddy covariance system consisted of one Gill Windmaster sonic anemometer (Gill Instruments Ltd., Lymington, Hampshire, United Kingdom) combined with the Microx TX3 using a tapered sensor, while for P5 the Gill sonic was replaced by a CSAT3 (Campbell Scientific, North Logan, Utah). In addition an open-path gas analyzer, LI-7500 (LI-COR Inc., Lincoln, Nebraska), was installed to determine the fluxes of CO_2 and humidity (Fig. 1). The eddy covariance (EC) system was mounted and evaluated at two different heights, 10 and 27 m. The sensor comparison test was performed at 10-m height (OI sensor), while data used for spectral and cospectral comparison with CO_2 and humidity were performed at 27-m height. The instruments were mounted at the outermost part of a 3.5-m bar attached to the tower facing south. The oxygen sensor was mounted to one of the supporting legs of the sonic anemometer, and the LI-7500 was mounted 0.35 m horizontally apart from the sonic anemometer with the detection volume in-line with the detection volume of the sonic. The thermistor of the Microx TX3 was mounted within the tower inside a ventilated radiation shield. The sampling rate of the EC system was set to 20 Hz. To get the best possible temporal resolution, the Microx TX3 was set to operate in "fast sampling" mode, which means the fastest possible update of the analog signal corresponding to about 2 Hz. Since the sampling rate for the EC system is larger compared to the analog update frequency of the Microx TX3, data in between updates were kept at a constant sample value. Prior to every new measuring period, a manual two-point calibration was performed on the oxygen sensor: the first point for 100% air saturation (in air) and the second point for 0% air saturation (in liquid).

4. Measurements

a. Data analysis

The details of atmospheric conditions during the measuring periods are presented in Table 2. To avoid disturbance from land and flow distortion effects from the tower, only data with a prevailing wind direction from the sector 60°–250° were used, for spectral analysis data were filtered to 80°–160° in order to represent open sea conditions for all scalars. Periods of rain and high relative humidity (>93%) were excluded by using the relative humidity measured at 8 m. Oxygen data were first screened to exclude periods of low signal-to-noise ratio, identified using the ratio of the oxygen fluctuation

and the tabulated precision of 0.1% air saturation. For sonic wind data, a rotation of the coordinate system was performed, by aligning the sonic x axis into the mean wind and a second rotation giving a zero vertical wind speed. Spectral analysis and turbulence statistics were compiled in 30-min blocks. For every 30-min block, the 10-min average wind directions are allowed to vary within ±10°, to ensure a persistent wind direction. To remove trends affecting the scalar averages, a linear detrend was applied on the raw data for every 30-min block. Time lags were checked by cross-correlating signals on every 30-min block in order to get the most accurate flux estimation. The time lag between oxygen and w was found to be zero. For w–CO_2 and w–q having a distance to the sonic of 0.35 m, a time lag of ±0.6 s was found, depending on wind speed and wind direction. A spike removal algorithm similar to Sahlée et al. (2012) was then conducted on the remaining data used for cospectral analysis.

b. Corrections

1) Air density effects

Density variations due to sensible and latent heat fluxes are known to affect open-path gas analyzers, such as the LI-7500, measuring the CO_2 molar density in ambient air within the given detection volume. Fluctuations of temperature and humidity cause fluctuations in the measured density, which need to be corrected for. A similar correction is needed also for the oxygen measurement presented here. The Microx TX3 measures the phase angle shift as a function of the partial pressure of oxygen in ambient air. As a result, the measured O_2 fluxes cannot be used directly without correcting for the effect of temperature and humidity fluctuations. The correction can be made directly on the raw data by converting the fluxes into mixing ratios as is done in Sahlée et al. (2008) for carbon dioxide or in the postprocessing using the WPL correction (Webb et al. 1980). The WPL correction is described by the following equation for the true vertical mass flux F_x (kg m^{-2} s^{-1}) of an in situ–measured mass scalar density ρ_x (kg m^{-3}):

$$F_x = \overline{w'\rho_x'} + \mu(\overline{\rho}_x/\overline{\rho}_a)\overline{w'\rho_v'} + (1+\mu\sigma)(\overline{\rho}_x/\overline{T})\overline{w'T'}. \quad (8)$$

The $\overline{w'\rho_x'}$ term denotes the measured density flux, the $\mu(\overline{\rho}_x/\overline{\rho}_a)\overline{w'\rho_v'}$ term is the contribution from the latent heat flux, and the $(1+\mu\sigma)(\overline{\rho}_x/\overline{T})\overline{w'T'}$ term is the part accounting for the sensible heat flux. Here σ is the ratio of water vapor density to the density of ambient air $\overline{\rho}_x/\overline{\rho}_a$ and μ is the ratio M_d/M_v, where M is the molar mass (kg mol^{-1}) where subscripts d, a, and v refer to dry air, ambient air, and water vapor, respectively. The Microx TX3 compensate for temperature fluctuations on a temporal scale above 20 s with the thermistor connected. Therefore, the oxygen flux should only be corrected with respect to the contribution from the latent heat flux [second term on the right-hand side in Eq. (8)] and if necessary, also with the contribution from the part of the sensible heat flux found below 20 s.

2) Flux estimation from spectral attenuated signals

The most frequently used method to determine the air–sea flux of oxygen is Eq. (4). However, when a correction due to limitations in frequency response is needed, the interpolated cospectrum Eq. (7) is preferably used. To compensate for the frequency loss, different methods have been suggested, such as different transfer functions developed for spectral attenuation (Horst 2000) or using in situ measurements and assuming cospectral similarity of a reference signal shown to be free from attenuation (Hicks and McMillen 1988; Horst et al. 1997). The transfer functions are usually smooth curves based on field measurements over flat terrain (Moore 1986; Kaimal and Finnigan 1994); however, as showed in several studies (Laubach and McNaughton 1998; Massman 2000, 2001) and summarized in Lee et al. (2004), half-hour spectra never resemble this smooth shape and the nondimensional frequencies were shown to be site specific rather than universal, causing errors in the transfer functions.

In this study the cospectral similarity was applied using nC_{wq} as the reference. The oxygen flux was determined by computing the integral of the oxygen cospectra up to the frequency where the flux loss starts (n_l). The flux contribution at frequencies higher than n_l is determined from the cospectra of the reference signal c multiplied by the ratio of the oxygen flux to the scalar flux up to the drop-off frequency:

$$F_o = \int_{-\infty}^{n_l} C_{wo}(n)\,dn + \frac{\int_{-\infty}^{n_l} C_{wo}(n)\,dn}{\int_{-\infty}^{n_l} C_{wc}(n)\,dn}\left[\int_{n_l}^{\infty} C_{wc}(n)\,dn\right]. \quad (9)$$

5. Results and discussion

a. Sensor comparison

In this section sensor and instrument limitations in terms of response time, signal drift, and flux detection limit are studied. Both the OI type and the NOI type of sensors were used. The measurements with the OI sensor were performed at P1, while measurements with the NOI sensor were performed during four field campaigns

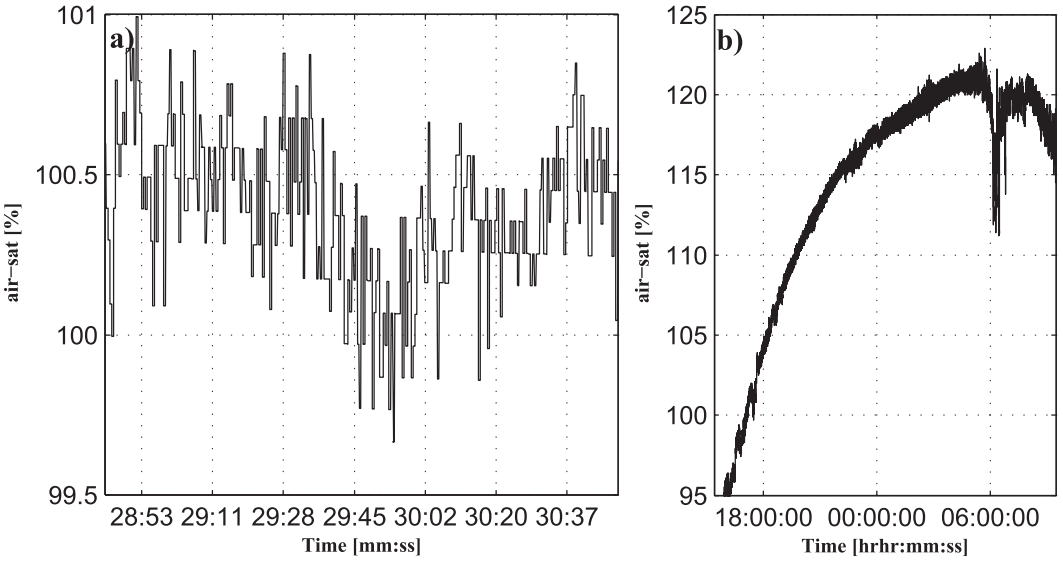

FIG. 2. Time series (LST) of oxygen raw data in % air saturation measured at the height of 27 m during P2: (a) 50-s series displaying the discrete behavior of the oxygen signal and (b) 17-h series showing the large signal drift (3.7 % airsaturation h^{-1}) of the NOI sensor.

over the years 2011–13. Figure 2a shows a detrended time series of the O_2 measurements with the NOI sensor during 30 June 2011. Both large-scale and small-scale fluctuations are observed; additionally, it is clear that the sensor displays a discrete stepwise response. The Microx TX3 shows this discrete signal regardless of the sensor tip used. However, as displayed in Fig. 2a, fluctuations of the order of 0.5% air saturation are detected within 30-s interval between 2925 and 2955 LST, and can be distinguished from the typical precision error of ±0.1% air saturation. This is most likely due to the combination of the limited resolution and the oversampled system (sampling at 20 Hz but the sensor outputs only at about 2 Hz). For eddy covariance measurement in water, the stepwise behavior was shown to have a minor effect on the calculated fluxes (Chipman et al. 2012). However, this does not necessary have to be the case for atmospheric eddy covariance measurements of oxygen where the concentration fluctuations are small relative to the absolute concentration.

For all field campaigns, a nonphysical trend in oxygen signal was seen as an increase in oxygen concentration with time (Fig. 2b). This trend in oxygen concentration starts immediately after a new sensor tip has been installed and measurements started. Figure 2b shows a time series of oxygen concentration measured during P2 with a new two-point calibrated NOI sensor tip installed. Regardless of the type of sensor tip, a signal drift could be distinguished; however, this signal drift was found to be much larger for the nonoptical isolated sensor than for the isolated sensor tip, sometimes as large as 3.7% air saturation per hour (Fig. 2b). This drift has not been recognized for use in aquatic environments (Chipman et al. 2012) and is probably due to photobleaching of the sensor tip (Loligo Systems 2005. The drift in oxygen signal could, if not reduced to its minimum, potentially have large influences on the computed oxygen fluxes. The impact from the drift on the oxygen flux is investigated by comparing the evolution of the oxygen flux [difference in flux compared to the initial flux $F_o(t) - F_o(0)$] with the evolution of the partial pressure of oxygen $P_o(t) - P_o(0)$ (Fig. 3a). The oxygen partial pressure increases with 35 hPa due to the drift. The signal drift is largest in the beginning of the measuring period and levels out after about 40 h; therefore, most of the data are found for $P_o(t) - P_o(0) > 20$ hPa. From $P_o(t) - P_o(0) = 15$ to 33 hPa, a small tendency is found for increasing oxygen fluxes. This is, however, more likely explained by natural trends in dynamical or biological forcing affecting the magnitude of the oxygen flux rather than the signal drift. For air–sea oxygen fluxes over such a relatively short period of time, dynamical forcing from wind speed is assumed to be the most important parameter affecting the magnitude of the oxygen flux.

During P5 the oxygen fluxes for the sector 80°–160° are found within the range 0.3–6.6 μmol m^{-2} s^{-1}, where the variation is mostly due to variations in wind speed. These oxygen fluxes are somewhat larger than the modeled 50-yr average oxygen flux for June of 0.6 μmol m^{-2} s^{-1} for the eastern Gotland basin (Norman et al. 2013). However, prior to evaluating the magnitude of the absolute air–sea scalar flux, several corrections need to be applied

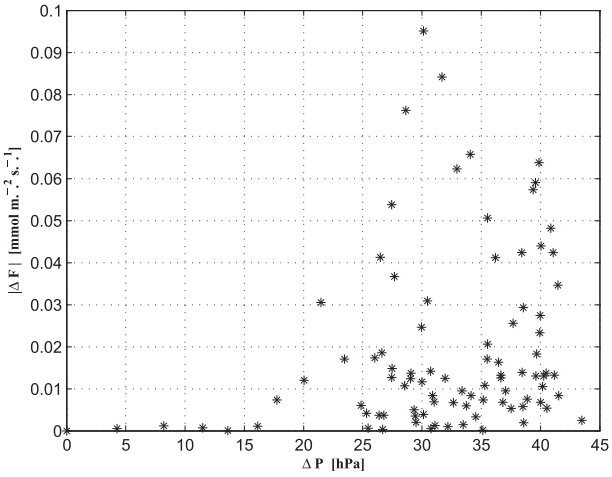

FIG. 3. Scatterplot of the evolution of the absolute value of the oxygen flux with time $F_o(t) - F_o(0)$, denoted by ΔF, showed against the evolution of the partial pressure of oxygen $P_o(t) - P_o(0)$, denoted by ΔP during P5.

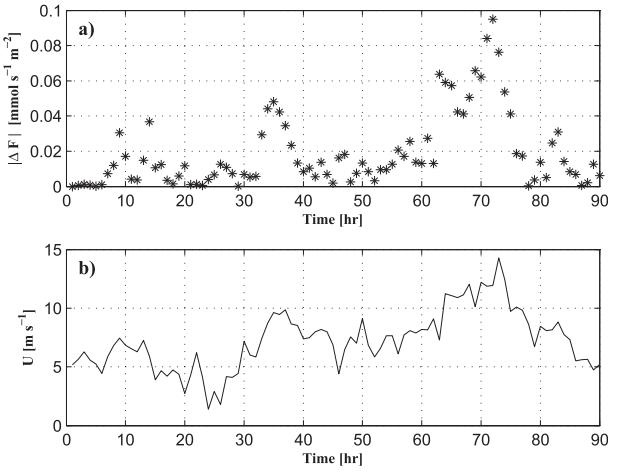

FIG. 4. Time series of (a) the absolute value of $F_o(t) - F_o(0)$, denoted by ΔF during P5, and (b) the 10-min mean horizontal wind speed at the height of 27 m during P5.

and flux uncertainty determined (Blomquist et al. 2010; Rowe et al. 2011; Yang et al. 2013); additionally, the air–sea scalar gradient needs to be verified by measurements. Here the oxygen fluxes are corrected according to Eq. (9) and for the contribution from the latent heat flux [second term on the right-hand side in Eq. (8)] affecting the measured density flux. In Fig. 4a the evolution of the absolute value of $F_o(t) - F_o(0)$ is shown as a function of time, and Fig. 4b shows the wind speed during the period. After about 30 h, the wind starts to increase from 5 m s^{-1} to reach its maximum of 14 m s^{-1} at 72 h after deployment. For most cases the large increase in oxygen flux coincides with high wind speeds, showing wind speed to be the dominant forcing on the oxygen flux rather than the influence from the signal drift.

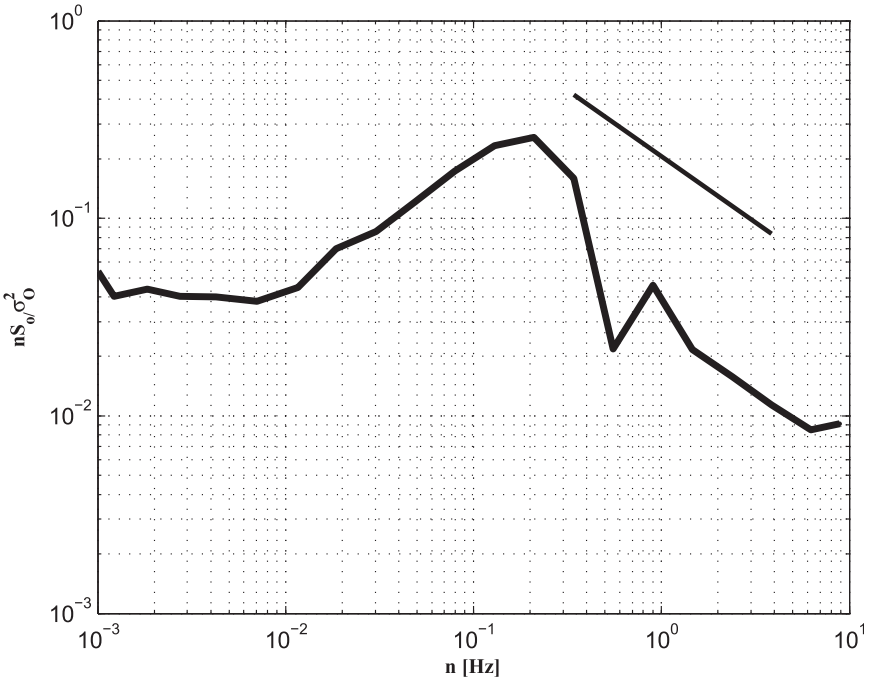

FIG. 5. Normalized mean power spectra of oxygen measured with the OI sensor plotted against frequency consisting of 14 consecutive half hours of data during P1 at 10-m height. Straight line indicates a $-2/3$ slope.

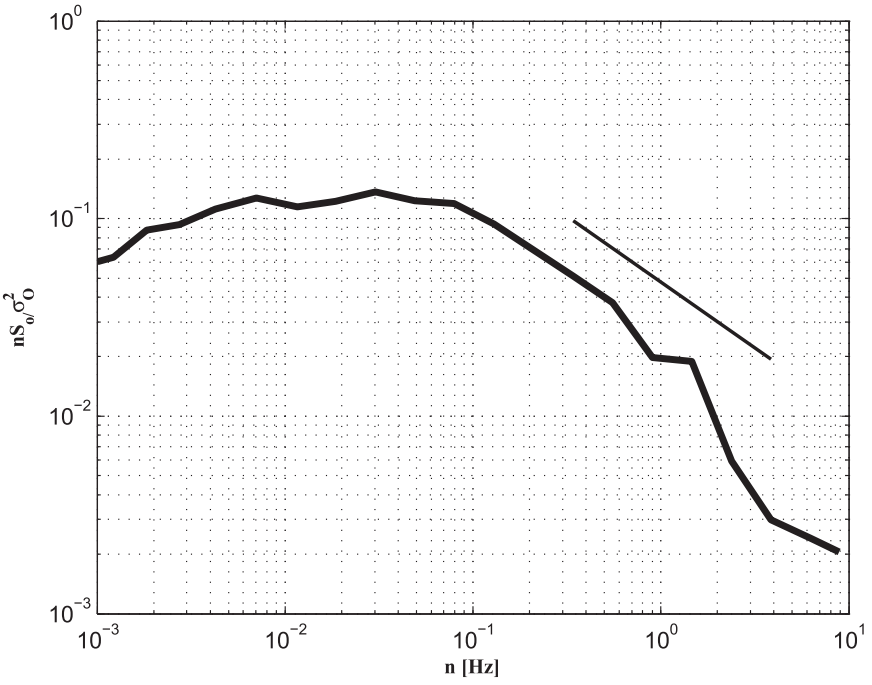

FIG. 6. Normalized mean power spectra measured with the NOI sensor plotted against frequency. The spectra is averaged over 50 half hours of data from 29 to 30 Aug 2012 at a height of 27 m. Straight line indicates a $-2/3$ slope.

To ascertain the most suitable oxygen sensor for eddy covariance measurements, normalized mean oxygen spectra of the OI sensor (Fig. 5) and the NOI sensor (Fig. 6) as a function of frequency are studied. The mean spectra in Fig. 5 consist of 14 half-hour runs measured with the OI sensor during P1. In agreement with the Kolmogorov theory for other scalars, oxygen spectra show a slope close to $-2/3$ in the inertial subrange; however, for frequencies higher than 0.3 Hz, a sudden drop in energy can be seen for the OI sensor. The energy loss occurs at frequencies higher than 0.3 Hz, which is slightly lower than what is to be expected for the OI sensor, which, according to the specification is capable of resolving eddies of sizes up to 0.5 Hz. The normalized oxygen power spectra for the NOI sensor (Fig. 6) represent an average of 50 half-hour runs measured during conditions close to neutral. The NOI sensor shows a slope close to $-2/3$ up to about 1 Hz, with a small tendency of a more spiky structure of the spectra in the range 0.5–1 Hz. After 1 Hz a drastic drop in oxygen power spectra is observed, indicating a response limited to 1 Hz, which corresponds to the tabulated response time of 0.5 s for the NOI sensor. Energy in the frequency range 1.0–10 Hz should be regarded as noise, since the update rate of the instrument is limited to 2 Hz. As expected there is a shift in the spectral peak frequency toward lower frequencies when measuring at 27-m height compared to 10-m height, which makes it possible to resolve a larger part of the spectrum, shown in Figs. 5 and 6.

Verification of the accuracy and stability of the oxygen instrument is of importance before using it for eddy covariance measurements. A shift in signal stability is observed for all individual sensors, appearing as a drastic impairment of the resolution of the oxygen sensor, causing errors in the determination of O_2 fluxes. To assure the sensor stability of the Microx TX3 with time, a signal inspection is needed before the calculation of oxygen fluxes. The signal stability may be evaluated using the normalized standard deviation, which should be a function of z/L only (Monin 1962):

$$\frac{\sigma_x}{x_*} = F_o\left(\frac{z}{L}\right), \tag{10}$$

where σ_x denotes the variance; $x_* = -\overline{w'x'}/u_*$ denotes the scaling parameters for the scalar; $u_* = \sqrt{-\overline{u'w'}}$ is the friction velocity; and z/L is the Monin–Obukhov stability parameter, where z denotes the measuring height and L is the Obukhov length defined as $L = -u_*^3 T/g\kappa w' T_v'$, where g is the gravity, κ is the von Kármán constant equal to 0.4, and T_v denotes the virtual temperature defined as $T_v = (1 + 0.61q)T$. Because of the limited dataset, the stability function $F_o(z/L)$ cannot be determined and Eq.

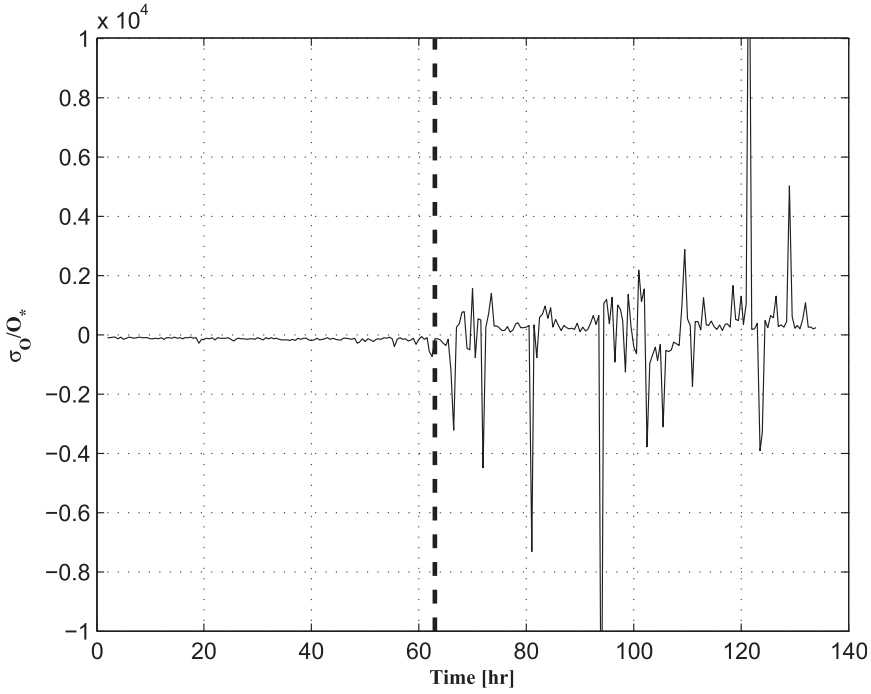

FIG. 7. Half hour average of σ_o/O_* plotted against hour record number during P4. The large fluctuation starting at record 62 marked by the dashed vertical line indicates a possible problem with the sensor.

(10) not be used directly. However, during P3–P5 only minor changes in z/L are measured and the dimensionless stability function $F_o(z/L)$ can be regarded as relatively constant. The ratio σ_o/O_* should then stay relatively constant as long as the oxygen sensor is capable of detecting true fluctuations of oxygen. Figure 7 displays 268 consecutive half hours of data with σ_o/O_* for near-neutral conditions during P4. After about 2.5 days (125 half hours), a drastic impairment of the oxygen sensor is observed, appearing as a threshold value in the oxygen signal, after which large variations begin, indicating that the oxygen sensor is no longer capable of detecting the true fluctuations of oxygen. This threshold value has showed to vary between sensors, depending on weather conditions, where strong sunlight tends to have a negative effect on the sensor lifetime (SL). Direct impact from raindrops, snow, and hail on the sensor tip has showed to directly reduce the sensor lifetime. Wintertime measurements have not yielded any good results, and are therefore not included in the study. Significant shifts in the oxygen signal affecting the ratio σ_o/O_* may also be due to other reasons, such as change in wind velocity or atmospheric stability. Therefore, a manual inspection of spectra and cospectra is recommended for periods when the ratio shows large deviations. To maximize in field data coverage continuous evaluation of the oxygen data through a control algorithm is recommended.

b. *Spectral analysis*

As previously discussed the peak frequency is shifted toward lower frequencies when measuring at 27-m height compared to 10-m height, meaning that the NOI sensor resolves a larger part of the spectra and cospectra. Because of scalar similarity, we expect the cospectra of oxygen to behave similar as the cospectra for CO_2 and humidity following a $-4/3$ slope within the inertial subrange, as in Sahlée et al. (2008), where the cospectra of CO_2 and humidity showed a similar shape. Mean cospectra of oxygen (blue), humidity (green), and CO_2 (red), normalized with the respective covariance [Eq. (4)] shown against dimensionless frequency, $f = nz/u$, measured at the height of 27 m, are shown in Figs. 8a and 8b. The normalized mean cospectra consist of the 22 half-hour runs during 30 August 2012. Overall, a good agreement between normalized oxygen cospectra and normalized cospectra of wq and wCO_2 is found up to f equal to 1, following a $-4/3$ slope in the inertial subrange. However, for oxygen a frequency loss compared to CO_2 and humidity can be distinguished already at f equal to 0.3, increasing dramatically above f equal to 1 where the slope no longer follows the $-4/3$ line. Figure 8b shows the normalized cospectra on a linear scale as a function of normalized frequency on a logarithmic scale.

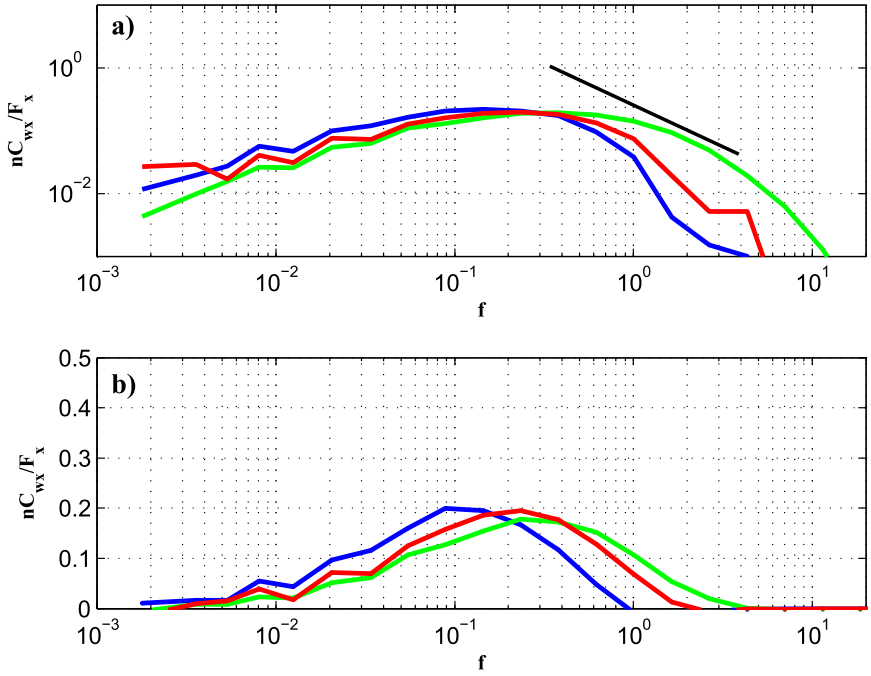

FIG. 8. Normalized mean cospectra of oxygen (blue), humidity (green), and CO_2 (red) plotted against normalized frequency: (a) in a log–log representation and (b) in a linear–log representation. The mean cospectra contain 22 half hours of data from 30 Aug 2012. Straight black line in (a) indicates a $-4/3$ slope.

As mentioned previously the area enclosed by the curve is proportional to the flux. For lower frequencies the normalized cospectra follow each other as expected. For higher frequencies, however, the cospectrum of oxygen is found to be consistently lower compared to cospectra of humidity and CO_2. For $f > 1$, the nC_{wo} cospectrum is found to be zero. However, less than 1% of the total fluxes of CO_2 and water vapor are associated with eddies in this range. The total loss in the normalized oxygen cospectra compared to the normalized cospectra of humidity and CO_2 is of importance for the magnitude of the total oxygen flux. To correct for this loss, the normalized cospectral shape of CO_2 and humidity or any other scalar can be used as the true shape of the normalized oxygen cospectra for frequencies higher than the drop-off frequency [cf. section 4b(2)].

c. *Corrections of O_2 fluxes*

Using the normalized mean cospectra of CO_2 and humidity, the oxygen flux is corrected by applying Eq. (7). The correction on the oxygen flux is (for cospectra in Fig. 8) 16% and 26% using nC_{wCO_2} and nC_{wq} as references, respectively. Expanding the measuring period to 48 half hours, the average cospectral correction constitutes 25% of the flux with individual half-hour cospectral corrections varying between 17% and 36% of the flux, using nC_{wq} as a reference. Figure 9 display 50 half hours of data during a 33-h period from 29 to 30 August; the red line shows the best fit to the data by the least squares method. As expected the cospectral correction always shows a positive contribution to the flux being above the blue line, representing a 1:1 relation between the corrected and the uncorrected oxygen flux. The curve

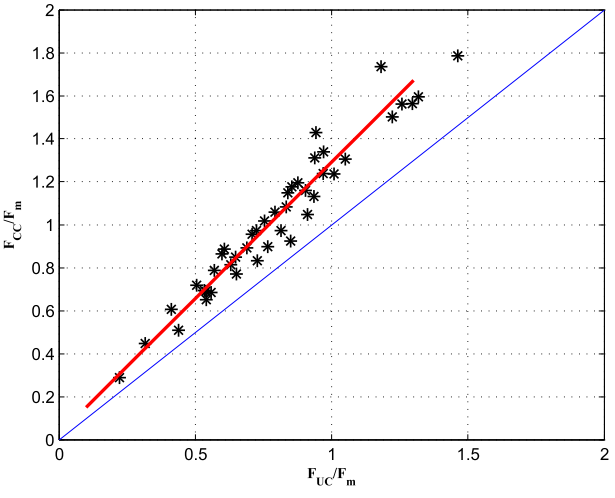

FIG. 9. Cospectral corrected flux (F_{CC}) normalized with the mean flux (F_m) for 50 half hours as a function of uncorrected flux (F_{UC}) normalized during P4. Red line displays the best curve fitting by the least squares method. Blue line shows the 1:1 relation between corrected and uncorrected flux.

representing the cospectral correction is a linear function with a slope of 1.27 (red line), indicating a relative constant value of the cospectral correction, with a small tendency of having larger cospectral correction for larger measured oxygen fluxes. The latent heat correction (LHC) part of the WPL correction was found to have the largest influence on the oxygen fluxes, showing a mostly positive contribution to the oxygen flux. The mean contributions from LHC during P4 were found to be 41% of the oxygen flux varying within the range 30%–74% of the oxygen flux.

6. Summary and conclusions

Using high-frequency oxygen data from the Östergarnsholm site, we show that the Microx TX3 with the nonoptical isolated (NOI) sensor attains sufficient response time and precision to be used in the eddy covariance system at 27 m to measure larger air–sea fluxes of O_2. The optical isolated (OI) sensor shows a more stable signal than the NOI sensor in terms of signal drift, not shown here; however, the slow response time of the OI sensor makes it insufficient for ground-based eddy covariance measurements. The signal drift of the NOI sensor will result in errors in the flux estimation if not corrected. This drift can be reduced by regular calibration and by lowering the sensor's light-emitting diode (LED) intensity; however, a lower LED intensity will also decrease the instrumental resolution, which is already a limitation for this instrument. This study reveals a significant limitation in sensor lifetime for the NOI sensor, which limits the application of the Microx TX3 in atmospheric eddy covariance systems. The sensor lifetime varied between 1 and 4 days, where the variations in sensor lifetime were found to depend on atmospheric conditions, such as solar radiation and direct impact from precipitation. We therefore encourage a signal stability control like the one presented in this study to select periods of data used for further analysis, and if necessary a manual spectral–cospectral inspection. To reduce the forcing on the oxygen sensor, land-based measurements are preferred where motions of the EC system are minimized.

Spectra of oxygen measured with the NOI sensor follow a $-2/3$ slope within the inertial subrange; however, above 1.0 Hz a pronounced drop in frequency response is seen. This study also reveals the importance of measuring at the highest possible altitude for instruments with a limited response time, such as the Microx TX3. Comparing normalized cospectra of oxygen, humidity, and CO_2 shows that they coincide and follow a $-4/3$ slope up to a normalized frequency > 1; thus, scalar similarity applies for oxygen on that part of the cospectrum during neutral conditions, measured with the Microx TX3 in combination with the NOI sensor. The frequency loss starting at $f > 0.3$ as a result of the limited resolution causes an underestimation of the oxygen flux. This flux loss can be corrected for either by a transfer function or as in this study applying cospectral similarity for scalars and using simultaneous high-frequency measurements of other scalars. The correction is performed upon the normalized cospectra by using the shape of the scalar as the reference shape of the normalized oxygen cospectra for frequencies higher than the frequency where the drop-off begins. This cospectral correction was found to be of significant importance for the magnitude of the total flux during P4 varying between 17% and 36% of the total oxygen flux. The magnitude of the cospectral correction during P4 showed a small increase with increasing oxygen fluxes. For periods with small air–sea gradients and strong stable atmospheric stratification, it is likely that the limitations in instrument regarding resolution and response time could result in large cospectral corrections and poorly quantified oxygen fluxes. The latent heat correction was found to have a large influence on the oxygen fluxes. During P4 LHC constituted 30%–74% of the flux and was likely to show an even larger influence for periods of high latent heat fluxes. Even though the latent heat correction corresponds to a major part of the oxygen flux, it has a solid theoretical base and is required for measurements with effectively open-path instruments in atmospheric EC systems and prior estimation of the scalar flux. For the situation when the density correction becomes very large, however, the oxygen flux can be questionable. We thus conclude that the Microx TX3 can be used for high-frequency purposes during the spring and summer months. However, the thermistor does not attain a sufficient response time for atmospheric applications; therefore, it would be further improved with a high-frequency thermistor.

Acknowledgments. We would like to give a special thanks to the anonymous reviewers for their most valuable feedback. We also thank all the people involved in the field campaigns and especially Eva Podgrajsek, for her technical assistance.

REFERENCES

Anderson, D. E., and S. B. Verma, 1985: Turbulence spectra of CO_2, water vapor temperature and wind velocity fluctuations over a crop surface. *Bound.-Layer Meteor.,* **33,** 1–14, doi:10.1007/BF00137033.

Arrigo, K. R., 2005: Marine microorganisms and global nutrient cycles. *Nature,* **437,** 349–355, doi:10.1038/nature04159.

Aubinet, M., T. Vesala, and D. Paple, Eds., 2012: *Eddy Covariance: A Practical Guide to Measurement and Data Analysis.* Springer Atmospheric Sciences Series, Springer, 436 pp.

Berg, P., H. Røy, F. Janssen, V. Meyer, B. Jørgensen, M. Huettel, and D. de Beer, 2003: Oxygen uptake by aquatic sediments measured with a novel non-invasive eddy-correlation technique. *Mar. Ecol. Prog. Ser.,* **261,** 75–83, doi:10.3354/meps261075.

——, R. N. Glud, A. Hume, H. Stahl, O. Kazumasa, V. Meyer, and H. Kitazato, 2009: Eddy correlation measurements of oxygen uptake in deep ocean sediments. *Limnol. Oceanogr. Methods,* **7,** 576–584, doi:10.4319/lom.2009.7.576.

Blomquist, B. W., C. W. Fairall, B. J. Huebert, D. J. Kieber, and G. R. Westby, 2006: DMS sea-air transfer velocity: Direct measurements by eddy covariance and parameterization based on the NOAA/COARE gas transfer model. *Geophys. Res. Lett.,* **33,** L07601, doi:10.1029/2006GL025735.

——, B. J. Huebert, C. W. Fairall, and I. C. Faloona, 2010: Determining the sea-air flux of dimethylsulfide by eddy correlation using mass spectrometry. *Atmos. Meas. Tech.,* **3,** 1–20, doi:10.5194/amt-3-1-2010.

Brand, A., D. F. Mcginnis, B. Wehrli, and A. Wueest, 2008: Intermittent oxygen flux from the interior into the bottom boundary of lakes as observed by eddy correlation. *Limnol. Oceanogr.,* **53,** 1997–2006, doi:10.4319/lo.2008.53.5.1997.

Chipman, L., M. Huettel, P. Berg, V. Meyer, I. Klimant, R. Glud, and F. Wenzhoefer, 2012: Oxygen optodes as fast sensors for eddy correlation measurements in aquatic systems. *Limnol. Oceanogr. Methods,* **10,** 304–316, doi:10.4319/lom.2012.10.304.

Codispoti, L., J. Brandes, J. Christensen, A. Devol, S. Naqvi, H. Paerl, and T. Yoshinari, 2001: The oceanic fixed nitrogen and nitrous oxide budgets: Moving targets as we enter the anthropocene? *Sci. Mar.,* **65,** 85–105, doi:10.3989/scimar.2001.65s285.

Fairaill, C. W., J. E. Hare, J. B. Edson, and W. R. McGillis, 2000: Measurement and parameterization of air–sea gas transfer. *Bound.-Layer Meteor.,* **96,** 63–105, doi:10.1023/A:1002662826020.

Garbe, C. S., and Coauthors, 2014: Transfer across the air-sea interface. *Ocean-Atmosphere Interactions of Gases and Particles,* P. S. Liss and M. T. Johnson, Eds., Springer Earth System Sciences, 55–112, doi:10.1007/978-3-642-25643-1_2.

Hicks, B. B., and R. T. McMillen, 1988: On the measurement of dry deposition using imperfect sensors and in non-ideal terrain. *Bound.-Layer Meteor.,* **42,** 79–84, doi:10.1007/BF00119876.

Högström, U., 1996: Review of some basic characteristics of the atmospheric surface layer. *Bound.-Layer Meteor.,* **78,** 215–246, doi:10.1007/BF00120937.

——, and Coauthors, 2008: To what extent can we believe measurements on a land-based tower to represent upwind open sea conditions. *Boreal Environ. Res.,* **13,** 475–502.

Horst, T. W., 2000: On frequency response corrections for eddy covariance flux measurements. *Bound.-Layer Meteor.,* **94,** 517–520, doi:10.1023/A:1002427517744.

——, S. P. Oncley, and S. R. Semmer, 1997: Measurement of water vapor fluxes using capacitance RH sensors and cospectral similarity. Preprints, *12th Symp. on Boundary Layers and Turbulence,* Vancouver, BC, Canada, Amer. Meteor. Soc., 360–361.

Joos, F., G. K. Plattner, T. F. Stocker, A. Körtzinger, and D. W. R. Wallace, 2003: Trends in marine dissolved oxygen: Implications for ocean circulation changes and the carbon budget. *Eos, Trans. Amer. Geophys. Union,* **84,** 197–201, doi:10.1029/2003EO210001.

Kaimal, J. C., and J. J. Finnigan, 1994: *Atmospheric Boundary Layer Flows*. Oxford University Press, 289 pp.

——, J. C. Wyngaard, Y. Izumi, and O. R. Coté, 1972: Spectral characteristics of surface layer turbulence. *Quart. J. Roy. Meteor. Soc.,* **98,** 563–589, doi:10.1002/qj.49709841707.

Karlsson, K., R. Rosenberg, and E. Bonsdorff, 2002: Temporal and spatial large-scale effects of eutrophication and oxygen deficiency on benthic fauna in Scandinavian and Baltic waters: A review. *Oceanogr. Mar. Biol.,* **40,** 427–489.

Keeling, R. F., A. Körtzinger, and N. Gruber, 2010: Ocean deoxygenation in a warming world. *Annu. Rev. Mar. Sci.,* **2,** 199–229, doi:10.1146/annurev.marine.010908.163855.

Kihm, C., and A. Körtzinger, 2010: Air-sea gas transfer velocity for oxygen derived from float data. *J. Geophys. Res.,* **115,** C12003, doi:10.1029/2009JC006077.

Körtzinger, A., U. Send, D. W. R. Wallace, J. Karstensen, and M. DeGrandpre, 2008: Seasonal cycle of O_2 and PCO_2 in the Labrador Sea: Atmospheric, biological, and physical implications. *Global Biogeochem. Cycles,* **22,** GB1014, doi:10.1029/2007GB003029.

Kuwae, T., K. Kamio, T. Inoue, E. Miyoshi, and Y. Uchiyama, 2006: Oxygen exchange flux between sediment and water in an intertidal sandflat, measured *in situ* by the eddy-correlation method. *Mar. Ecol. Prog. Ser.,* **307,** 59–68, doi:10.3354/meps307059.

Laubach, J., and K. G. McNaughton, 1998: A spectrum-independent procedure for correcting eddy fluxes measured with separated sensors. *Bound.-Layer Meteor.,* **89,** 445–467, doi:10.1023/A:1001759903058.

Lee, X., W. Massman, and L. Beverly, 2004: *Handbook of Micrometeorology*. Kluwer Academic Publishers, 245 pp.

Liss, P. S., and L. Merlivat, 1986: Air–sea gas exchange rates: Introduction and synthesis. *The Role of Air–Sea Exchange in Geochemical Cycling,* P. Buat-Menard, Ed., NATO Science Series C, Vol. 185, Springer, 113–127.

Loligo Systems, 2005: Microx TX3 fiber-optic oxygen meter. Instruction Manual, Software Version TX3v531, 96 pp. [Available online at http://www.loligosystems.com/getfile_d.php?id=4104.]

Massman, W. J., 2000: A simple method for estimating frequency response corrections for eddy covariance systems. *Agric. For. Meteor.,* **104,** 185–198, doi:10.1016/S0168-1923(00)00164-7.

——, 2001: Reply to comment by Rannik on ''A simple method for estimating frequency response corrections for eddy covariance systems.'' *Agric. For. Meteor.,* **107,** 247–251, doi:10.1016/S0168-1923(00)00237-9.

McGillis, W. R., and Coauthors, 2004: Air-sea CO_2 exchange in the equatorial Pacific. *J. Geophys. Res.,* **109,** C08S02, doi:10.1029/2003JC002256.

McGinnis, D. F., P. Berg, A. Brand, C. Lorrai, T. J. Edmonds, and A. Wuest, 2008: Measurements of eddy correlation oxygen fluxes in shallow freshwaters: Towards routine applications and analysis. *Geophys. Res. Lett.,* **35,** L04403, doi:10.1029/2007GL032747.

McNeil, C. L., and E. D'Asaro, 2007: Parameterization of air-sea gas fluxes at extreme wind speeds. *J. Mar. Syst.,* **66,** 110–121, doi:10.1016/j.jmarsys.2006.05.013.

——, B. Ward, W. R. McGillis, M. D. DeGrandPre, and L. Marcinowski, 2006: Fluxes of N_2, O_2, and CO_2 in nearshore waters off Martha's Vineyard. *Cont. Shelf Res.,* **26,** 1281–1294, doi:10.1016/j.csr.2006.04.008.

Monin, A. S., 1962: Empirical data on turbulence in the surface layer of the atmosphere. *J. Geophys. Res.,* **67,** 3103–3109, doi:10.1029/JZ067i008p03103.

Moore, C. J., 1986: Frequency response corrections for eddy correlation systems. *Bound.-Layer Meteor.,* **37,** 17–35, doi:10.1007/BF00122754.

Norman, M., A. Rutgersson, L. L. Sørensen, and E. Sahlée, 2012: Methods for estimating air–sea fluxes of CO_2 using high-frequency measurements. *Bound.-Layer Meteor.,* **144,** 379–400, doi:10.1007/s10546-012-9730-9.

——, ——, and E. Sahlée, 2013: Impact of improved air–sea gas transfer velocity on fluxes and water chemistry in a Baltic Sea model. *J. Mar. Syst.,* **111–112,** 175–188, doi:10.1016/j.jmarsys.2012.10.013.

Ohtaki, E., 1982: Kolmogorov constant for carbon dioxide in the atmospheric surface layer over a paddy field. *Bound.-Layer Meteor.,* **23,** 153–159, doi:10.1007/BF00123293.

——, 1985: On the similarity in atmospheric fluctuations of carbon dioxide, water vapor and temperature over vegetated fields. *Bound.-Layer Meteor.,* **32,** 25–37, doi:10.1007/BF00120712.

——, and T. Matsui, 1982: Infrared device for simultaneous measurement of fluctuations of atmospheric carbon dioxide and water vapor. *Bound.-Layer Meteor.,* **24,** 109–119, doi:10.1007/BF00121803.

Paulmier, A., D. Ruiz-Pino, and V. Garçon, 2008: The oxygen minimum zone (OMZ) off Chile as intense source of CO_2 and N_2O. *Cont. Shelf Res.,* **28,** 2746–2756, doi:10.1016/j.csr.2008.09.012.

Reimers, C. E., H. T. Özkan-Haller, P. Berg, A. Devol, K. McCann-Grosvenor, and R. D. Sanders, 2012: Benthic oxygen consumption rates during hypoxic conditions on the Oregon continental shelf: Evaluation of the eddy correlation method. *J. Geophys. Res.,* **117,** C02021, doi:10.1029/2011JC007564.

Rowe, M. D., C. W. Fairall, and J. A. Perlinger, 2011: Chemical sensor resolution requirements for near-surface measurements of turbulent fluxes. *Atmos. Chem. Phys.,* **11,** 5263–5275, doi:10.5194/acp-11-5263-2011.

Rutgersson, A., and A. Smedman, 2010: Enhanced air–sea CO_2 transfer due to water-side convection. *J. Mar. Syst.,* **80,** 125–134, doi:10.1016/j.jmarsys.2009.11.004.

——, M. Norman, B. Schneider, H. Pettersson, and E. Sahlée, 2008: The annual cycle of carbon dioxide and parameters influencing the air–sea carbon exchange in the Baltic Proper. *J. Mar. Syst.,* **74,** 381–394, doi:10.1016/j.jmarsys.2008.02.005.

——, A. Smedman, and E. Sahlée, 2011: Oceanic convective mixing and the impact on air–sea gas transfer velocity. *Geophys. Res. Lett.,* **38,** L02602, doi:10.1029/2010GL045581.

Sahlée, E., A. S. Smedman, A. Rutgersson, and U. Högström, 2008: Spectra of CO_2 and water vapour in the marine atmospheric boundary layer. *Bound.-Layer Meteor.,* **126,** 279–295, doi:10.1007/s10546-007-9230-5.

——, W. M. Drennan, H. Potter, and M. A. Rebozo, 2012: Waves and air-sea fluxes from a drifting ASIS buoy during the Southern Ocean Gas Exchange experiment. *J. Geophys. Res.,* **117,** C08003, doi:10.1029/2012JC008032.

Smedman, A., U. Högström, H. Bergström, A. Rutgersson, K. Kahma, and H. Pettersson, 1999: A case-study of air-sea interaction during swell conditions. *J. Geophys. Res.,* **104,** 25 833–25 851, doi:10.1029/1999JC900213.

Stern, O., and M. Volmer, 1919: Über die Abklingzeit der Fluoreszenz. *Phys. Z.,* **20,** 183–188.

Stigebrandt, A., 1991: Computations of oxygen fluxes through the sea surface and the net production of organic matter with application to the Baltic and adjacent seas. *Limnol. Oceanogr.,* **36,** 444–454, doi:10.4319/lo.1991.36.3.0444.

Stocker, T. F., and Coauthors, 2013: *Climate Change 2013: The Physical Science Basis.* Cambridge University Press, 1535 pp. [Available online at www.climatechange2013.org/images/report/WG1AR5_ALL_FINAL.pdf.]

Stramma, L., G. C. Johnson, J. Sprintall, and V. Mohrholz, 2008: Expanding oxygen-minimum zones in the tropical oceans. *Science,* **320,** 655–658, doi:10.1126/science.1153847.

——, and Coauthors, 2012: Expansion of oxygen minimum zones may reduce available habitat for tropical pelagic fishes. *Nat. Climate Change,* **2,** 33–37, doi:10.1038/nclimate1304.

Verma, S., and D. Anderson, 1984: Kolmogorov constants for CO_2, wind velocity, air temperature, and humidity fluctuations over a crop surface. *Bound.-Layer Meteor.,* **28,** 161–167, doi:10.1007/BF00119461.

Wanninkhof, R., 1992: Relationship between wind speed and gas exchange over the ocean. *J. Geophys. Res.,* **97,** 7373–7382, doi:10.1029/92JC00188.

——, and W. R. McGillis, 1999: A cubic relationship between gas transfer and wind speed. *Geophys. Res. Lett.,* **26,** 1889–1893, doi:10.1029/1999GL900363.

——, W. E. Asher, D. T. Ho, C. Sweeney, and W. R. McGillis, 2009: Advances in quantifying air-sea gas exchange and environmental forcing. *Annu. Rev. Mar. Sci.,* **1,** 213–244, doi:10.1146/annurev.marine.010908.163742.

Webb, E. K., G. I. Pearman, and R. Leuning, 1980: Correction of flux measurements for density effects due to heat water vapor transport. *Quart. J. Roy. Meteor. Soc.,* **106,** 85–100, doi:10.1002/qj.49710644707.

Woolf, D. K., 1993: Bubbles and the air–sea transfer velocity of gases. *Atmos.–Ocean,* **31,** 517–540, doi:10.1080/07055900.1993.9649484.

——, 1997: Bubbles and their role in air–sea gas exchange. *The Sea Surface and Global Change,* P. Liss and R. Duce, Eds., Cambridge University Press, 173–205.

——, 2005: Parameterization of gas transfer velocity and sea-state-dependent wave breaking. *Tellus,* **57B,** 87–94, doi:10.1111/j.1600-0889.2005.00139.x.

Wyngaard, J. C., 2010: *Turbulence in the Atmosphere.* Cambridge University Press, 393 pp.

——, and O. R. Cote, 1972: Cospectral similarity in the atmospheric surface layer. *Quart. J. Roy. Meteor. Soc.,* **98,** 590–603, doi:10.1002/qj.49709841708.

Yang, M., R. Beale, T. Smyth, and B. Blomquist, 2013: Measurements of OVOC fluxes by eddy covariance using a proton-transfer-reaction mass spectrometer—Method development at a coastal site. *Atmos. Chem. Phys.,* **13,** 6165–6184, doi:10.5194/acp-13-6165-2013.

Zappa, C. J., W. E. Asher, and A. T. Jessup, 2001: Microscale wave breaking and air-water gas transfer. *J. Geophys. Res.,* **106,** 9385–9391, doi:10.1029/2000JC000262.